

## RADIATIVE SHOCK-WAVE THEORY. I. CHEMICAL ABUNDANCE DIAGNOSTICS AND GALACTIC ABUNDANCE GRADIENTS

MICHAEL A. DOPITA,<sup>1</sup> LUC BINETTE,<sup>1</sup> SANDRO D'ODORICO,<sup>2</sup> AND PIERO BENVENUTI<sup>3</sup>

Received 1982 November 15; accepted 1983 June 23

### ABSTRACT

Using an extensive grid of fully radiative plane-parallel shock models, we have investigated how both the visible forbidden and UV intercombination lines may be used for chemical abundance diagnostics in supernova remnants. We find that, for shock velocities in excess of a critical value, the emergent spectrum depends primarily on abundance rather than on the shock conditions.

Available spectrophotometry confirms this conclusion, and we use the data to show, first, that the oxygen/nitrogen abundance ratio decreases by about a factor of 5 for a factor of 10 increase in oxygen abundance; second, that the oxygen/sulphur abundance seems constant at  $45 \pm 15$  from galaxy to galaxy; and third, that the abundance gradient in M31 is  $-0.05 \pm 0.02$  dex kpc<sup>-1</sup>.

*Subject headings:* nebulae: abundances — nebulae: supernova remnants — shock waves

### I. INTRODUCTION

It is now generally accepted that in evolved supernova remnants (SNRs) we see the spectral signature of a radiative shock wave propagating into denser regions of the interstellar medium (ISM). Over the last 7 years a large body of observational evidence has been collected about galactic and extragalactic SNRs which appears to show that the detailed spectra of these objects are primarily sensitive to the chemical abundances in the ISM rather than to the shock conditions (Dopita 1982). This is particularly well illustrated by the discovery of systematic line ratio variations in spiral galaxies which have been interpreted as due to galactic abundance gradients. These were first discovered in M33 (Dopita, D'Odorico, and Benvenuti 1980), have also been found in M31 (Blair, Kirshner, and Chevalier 1981, 1982; Dennefeld and Kunth 1981), and have recently been recognized in our Galaxy (Binette *et al.* 1982). Other galaxies either do not have enough SNRs to establish a gradient (D'Odorico, Dopita, and Benvenuti 1980; D'Odorico and Dopita 1983), or else, as in the LMC, gradients are absent (Dopita 1976; Dopita, Mathewson, and Ford 1977; Dopita, D'Odorico, and Benvenuti 1980). However, the global ensemble of spectrophotometric data shows clear evidence for a wide range of metallicity. This will be discussed below.

Up to the present, the interpretation of the observational material, in particular, the ability to disentangle the various influences of metallicity shock conditions and nonequilibrium effects on the optical spectra, has been hampered by the paucity of theoretical models in the literature. Nevertheless, our knowledge of the structure of steady-flow radiative shock waves has improved greatly since the pioneering work of Cox (1972), and many arbitrary assumptions have been lifted. Dopita (1976, 1977) and Raymond (1979) raised the assumption of collisional ionization equilibrium in the postshock gas. They also considered the transfer problem of UV photons generated in the hot plasma down through the recombination

zone. Shull and McKee (1979) constructed self-consistent models allowing for the diffusion of these same photons into the preshock region. The relaxation between electrons and ions in the postshock region of partially pre-ionized shocks has been considered by Ohtani (1980). The importance of charge transfer reactions other than  $O^0 + H^+ \rightleftharpoons O^+ + H^0$  and  $N^0 + H^+ \rightleftharpoons N^+ + H^0$  was assessed by Butler and Raymond (1980), and both Shull (1978) and Draine (1981) have considered the effects of dust on shock structure.

All of the above models have steady flow conditions and shock velocities ( $V_s$ ) less than 200 km s<sup>-1</sup>. Only the models of Dopita (1977) attempt to address the effect of metallicity on shock spectra in a systematic way. However, advances in modeling have rendered these models somewhat obsolete.

In the second paper of this series, we will describe in detail a new modeling code MAPPINGS and apply this to low-density steady-flow shocks of high velocity (Binette, Dopita, and Tuohy 1983, hereafter Paper II). This code incorporates all of the effects included in the earlier papers referenced above, also allows for Auger ionization and heating, contains a very large number of coolants, and predicts relative intensities of a large number of lines.

In this paper we apply this code to compute an extensive grid of models for fixed physical conditions appropriate to a typical evolved SNR, but allowing total abundances and abundance ratios of particular elements to vary over a sufficiently wide range so as to encompass all known spectrophotometry of evolved remnants. We then apply this grid to the observational data set.

### II. THE OBSERVATIONAL DATA BASE

Where SNRs in external galaxies have been observed (Dopita, D'Odorico, and Benvenuti 1980; D'Odorico and Dopita 1983; Blair, Kirshner, and Chevalier 1981, 1982; Dennefeld and Kunth 1981), the spectra usually extend from [O II]  $\lambda 3727$  to [S II]  $\lambda 6731$ . In principle then, each observational spectrum could be separately modeled by the shock code to give absolute abundances of He, N, O, Ne, and S. This has been done in a few cases (D'Odorico and Dopita 1983),

<sup>1</sup> Mount Stromlo and Siding Spring Observatories, Research School of Physical Sciences, Australian National University.

<sup>2</sup> European Southern Observatory, Garching-bei-München, FDR.

<sup>3</sup> ESA Villafranca, Satellite Tracking Station, Madrid, Spain.

but for those astronomers who do not have access to a general-purpose modeling code, this is not a viable solution. What we require, therefore, are general techniques and diagnostic grids whereby such data can be analyzed with sufficient accuracy. Such grids were computed by Dopita (1977) but did not cover the full range of abundances of interest. Before developing new grids, we now examine the data base to find whether systematic abundance effects are displayed in the spectrophotometry of SNRs in external galaxies.

The strongest lines in the visible spectra of SNRs, which have been unequivocally detected in all extragalactic SNRs are, apart from the Balmer lines of hydrogen, [O II]  $\lambda 3727$ , [O III]  $\lambda\lambda 4959, 5007$ , [N II]  $\lambda\lambda 6548, 6584$ , and [S II]  $\lambda\lambda 6717, 6731$ . The lines of [O I]  $\lambda\lambda 6300, 6363$  are frequently strong, but in low-dispersion spectra are confused with night-sky lines and are subject to a large measurement error. We therefore restrict our attention to the first four forbidden lines and their ratios with respect to nearby Balmer lines.

The [N II]  $\lambda\lambda 6548, 6584/H\alpha$  ratio is already known to be a rather good tracer of galactic abundance gradients, systematic trends with galactocentric distance having been found in M33 (Dopita, D'Odorico, and Benvenuti 1980), M31 (Blair,

Kirshner, and Chevalier 1981, 1982; Dennefeld and Kunth 1981), and in our own Galaxy (Binette *et al.* 1982).

The [S II] lines are, of course, subject to collisional de-excitation effects and are therefore more sensitive to physical conditions in the shock. Where both lines are used, the evidence for gradients is somewhat equivocal. However, most of the sensitivity to density can be removed by taking ratios with respect to the [S II]  $\lambda 6731$  line only, as the local density at which collisional effects become important for this line is reached for  $n_e \geq 10^4 \text{ cm}^{-3}$  (Pradham 1978). Such densities are reached in very few SNRs. Kepler is the most extreme case known (Leibowitz and Danziger 1983), and even here the local density only ranges as high as  $1.8 \times 10^4 \text{ cm}^{-3}$ .

In Figure 1 we plot the [N II]  $\lambda\lambda 6548, 6584/H\alpha$  ratio against the [S II]  $\lambda 6731/H\alpha$  ratio for all the SNRs cited above, with additional points for the galactic SNRs, RCW 86 (Ruiz 1981), RCW 103 (Dopita, D'Odorico, and Benvenuti 1980), and the Cygnus Loop (Fesen, Blair, and Kirshner 1982). There is a well-developed correlation between these two ratios, which cannot be caused by anything other than metallicity variations, since objects with strong [S II] also show strong [N II] and lie in the inner regions of the larger galaxies. SNRs in the

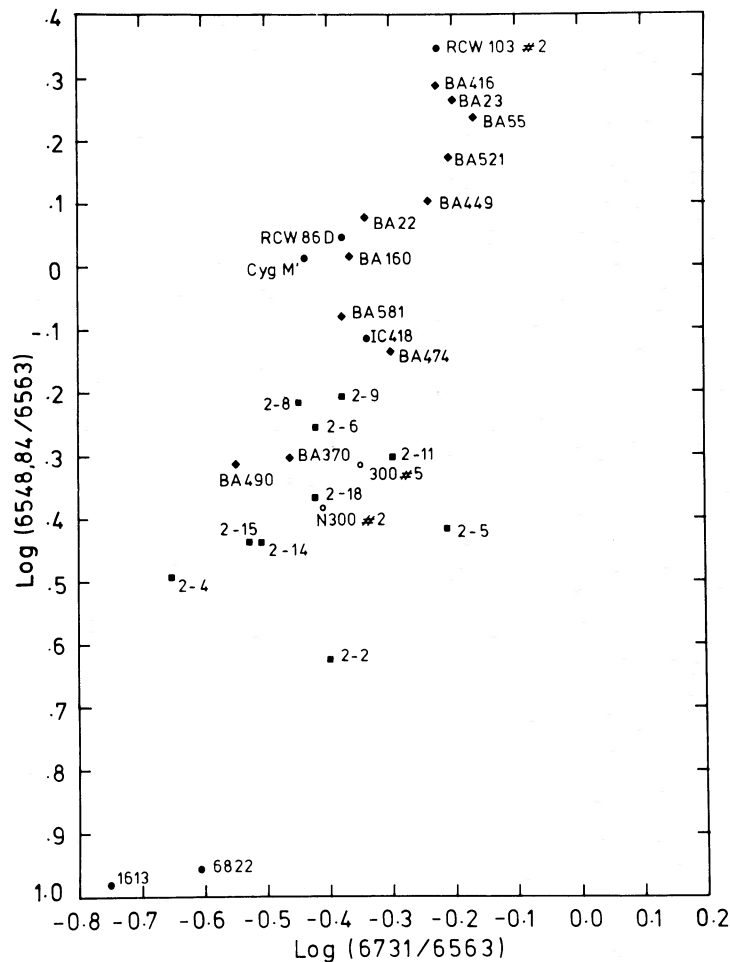


FIG. 1.—The relationship between the relative fluxes of the [S II]  $\lambda 6731$  and [N II]  $\lambda\lambda 6548, 6584$  lines with respect to  $H\alpha$  for global spectrophotometry of SNRs, showing abundance-dependent trends.

Magellanic irregular galaxies, on the other hand, show very weak forbidden lines by comparison. The size of the variation in  $[S II]/H\alpha$  is much smaller than the corresponding variation in  $[N II]/H\alpha$ , and there is some evidence of a "saturation" effect in the  $[S II]$  lines setting in at the strong line limit. This could be due to a variety of effects, which we discuss below.

If metallicity variations rather than physical conditions do in fact dominate the spectra of evolved SNRs, then there should also be a correlation between the  $[O II] \lambda\lambda 3727, 3729/H\beta$  ratio and the  $[O III] \lambda\lambda 4959, 5007/H\beta$  ratio. In an earlier paper (Dopita 1977) it was shown that the  $[O III]$  lines are particularly sensitive to shock conditions, since they originate in the hot plasma closer to the shock front than other lines in the optical spectrum, and the ionization conditions in this region depend critically on shock conditions. Figure 2 shows that the expected correlation exists in the data. However, there is again evidence for saturation, this time in the  $[O II]$  lines, since there is a strong tendency for SNRs to cluster at about  $\log(3727, 3729/4861) \approx 1.0$ .

The sensitivity of the  $[O III] \lambda\lambda 4959, 5007/H\beta$  ratio to the physical conditions can be better judged in Figure 3, where this ratio is plotted against the  $[N II] \lambda\lambda 6548, 6584/H\alpha$  ratio. Again,

a very clear correlation emerges, but the scatter is somewhat wider, about 0.25 dex.

These three figures, when taken together, constitute empirical evidence that the global spectrophotometry of SNRs gives a family of spectra which are primarily sensitive to the chemical abundances in the shocked plasma. The physical conditions in the shock appear to be of only secondary importance in determining the emergent spectra.

Our aim is to calibrate these empirical relationships.

### III. THE MODELS

#### a) Velocity-Dependent Effects

The physical content and method of solution of the models is described in Paper II of this series and will not be repeated here.

Our calculations are of steady-flow fully radiative shocks with a self-consistent pre-ionization (Shull and McKee 1979). The effects of disequilibrium are discussed elsewhere (Dopita and Binette 1983). In this type of model, the effect of the ionizing photons produced in the cooling zone of the shock is approximately allowed for by treating the ionizing precursor as a one-zone R-type ionization front. The ionization of *all*

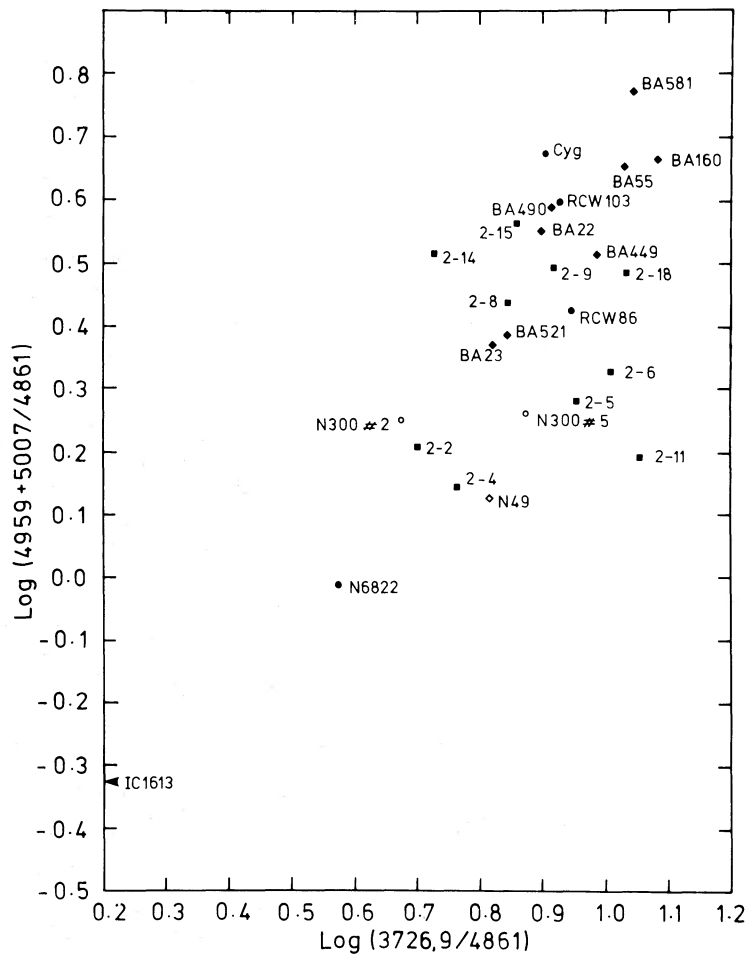


FIG. 2.—As Fig. 1 but for the  $[O II] \lambda\lambda 3726, 3729$  and  $[O III] \lambda\lambda 4959, 5007$  lines with respect to  $H\beta$

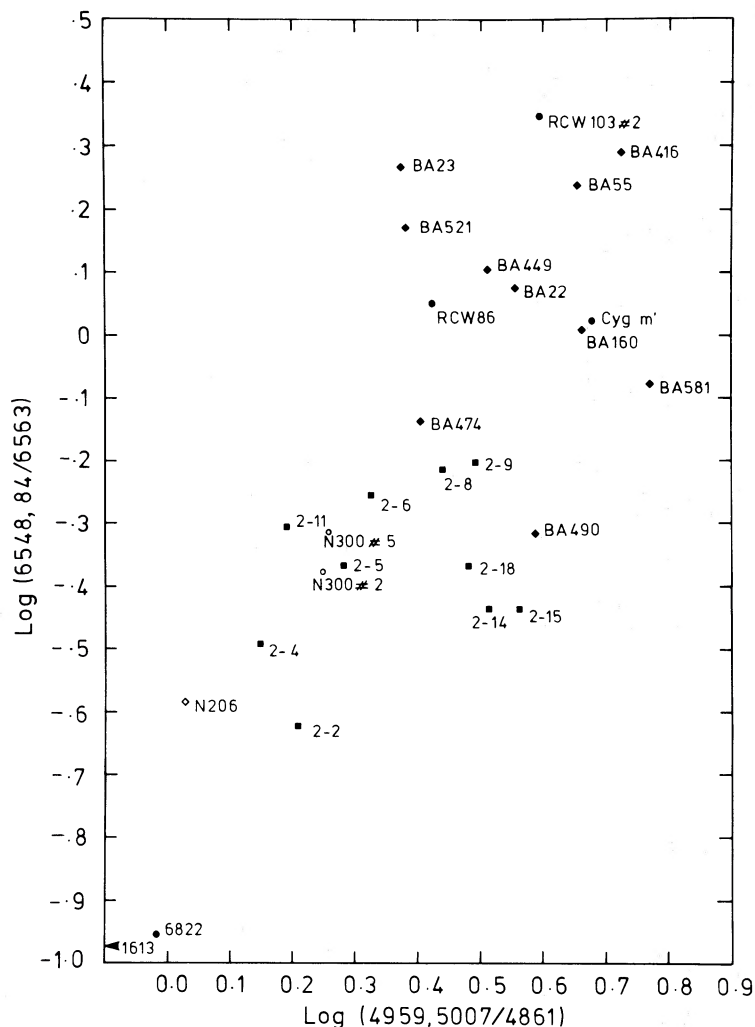


FIG. 3.—As Fig. 1 but for the  $[\text{O III}] \lambda\lambda 4959, 5007/\text{H}\beta$  ratio and the  $[\text{N II}] \lambda\lambda 6548, 6584/\text{H}\alpha$  ratio. The slope of the correlation is steeper than that expected if nitrogen was entirely primary.

ionic species by the radiation field is included in these calculations.

In order to compare our pre-ionization with previous models, we ran a low-density sequence of models with “cosmic” abundances (Allen 1973). Figure 4 shows the result for the fractional preionization of hydrogen, helium, and oxygen, which should be compared with Figure 5*b* of Shull and McKee (1979). Full pre-ionization of hydrogen is essentially reached at  $110 \text{ km s}^{-1}$  shock velocity in both models. However, we find a larger fractional pre-ionization at lower velocities, and a lower pre-ionization at the highest velocities. This is no doubt caused by our inclusion of more cooling processes and our different treatment of the radiative transfer problem for resonance line photons (see Paper II).

This sequence of models also serves the purpose of demonstrating the velocity-dependent effects on the emergent spectrum. Figure 5 shows how the ratios of the important forbidden lines (with respect to  $\text{H}\beta$ ) vary as a function of shock velocity. In the regime where hydrogen is fully pre-ionized, the variation with velocity is very small. This stability against shock conditions was demonstrated (in

Paper II) to persist up to a postshock temperature in excess of  $10^{5.7} \text{ K}$ , or a shock velocity larger than  $200 \text{ km s}^{-1}$ , and is one of the major reasons why SNR spectroscopy is such a promising tool as a probe of chemical abundances in the interstellar medium.

A second factor of importance is that for shock velocities high enough to provide significant pre-ionization of hydrogen ( $V_s \gtrsim 100 \text{ km s}^{-1}$ ), the emergent spectrum depends very little on details of the pre-ionization. To demonstrate this, we ran a sequence of models in which we took all elements in the preshock gas to be singly pre-ionized, regardless of shock velocity. Figure 6 is a plot similar to Figure 5 for these models. Although below  $V_s = 100 \text{ km s}^{-1}$  there are dramatic differences in line ratios between the two sets of models, above this velocity line ratios agree to within 0.1 dex.

At low velocities, the behavior of the  $[\text{O II}]$  and  $[\text{O III}]$  lines is particularly instructive. Note in Figure 5 the collapse of the  $\lambda 5007$  line intensity as the  $\text{O}^+$  species disappears from the preshock plasma. In the singly pre-ionized models, cooling is sufficiently slow to allow some  $\text{O}^+$  to  $\text{O}^{++}$  ionization, so that the  $\lambda 5007$  line declines slowly with decreasing shock

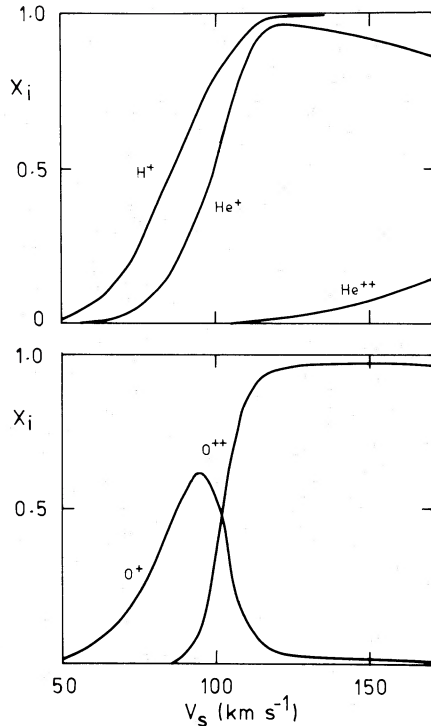


FIG. 4.—Self-consistent pre-ionization of H, He, and O in our models of standard abundance (Table 1). Compare with Shull and McKee (1979).

velocity, but in the self-consistent models, hydrogen collisional cooling dominates and reduces the postshock cooling time. This suppresses the further ionization of oxygen.

Since the oxygen ionization is locked to that of hydrogen by charge-exchange, in the singly ionized models the [O III] persists and even becomes stronger as the post shock temperature structure becomes more favorable to its emission.

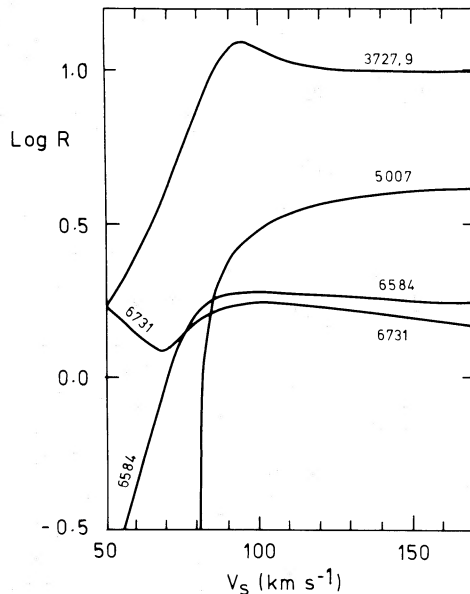


FIG. 5.—Line ratios,  $R$ , with respect to  $H\beta$  in fully self-consistent models of standard abundance (Table 1).

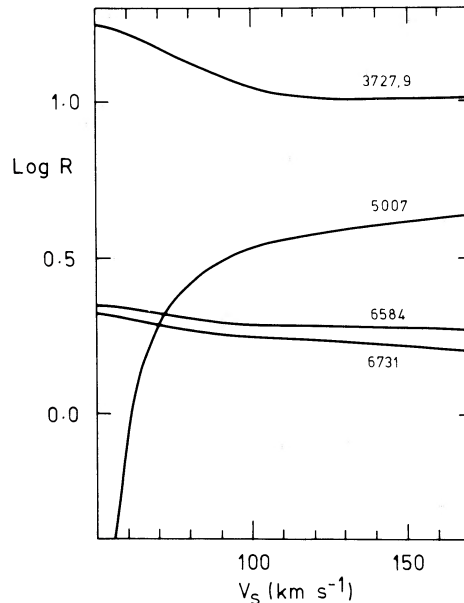


FIG. 6.—As Fig. 5 but for fixed pre-ionization (all elements singly ionized). Note that Figs. 5 and 6 are scarcely distinguishable for  $V_s \gtrsim 105 \text{ km s}^{-1}$ .

In the self-consistent models, however, it peaks at a point where the column relative abundance of the  $O^+$  ion is maximized, but it declines rapidly in relative intensity as hydrogen becomes un-ionized in the preshock gas, and collisional excitation of the Balmer lines becomes more important than recombination in determining hydrogen line intensities.

#### b) Abundance Effects on Optical Lines

Provided that hydrogen is pre-ionized, either by radiation produced within the cooling zone of the shock or by a stellar photon field, the results of the previous section confirm the empirical conclusion of § II: that shock conditions have only a secondary effect on the principal forbidden lines at optical wavelengths.

We can therefore proceed to investigate abundance effects on the emergent spectrum at a fixed set of physical conditions and have some degree of confidence that detailed modeling of individual remnants will give abundances that differ only slightly from those inferred from our grid of models.

We therefore arbitrarily choose a set of physical conditions for our grid and a set of initial abundances (in this case, those which give an emergent spectrum similar to SNRs in the solar neighborhood and are characterized by a mild depletion of refractory elements C, Mg, and Si). Our choice for the reference model is summarized in Table 1, and the output spectrum in Table 2.

A set of models is generated with a fixed relative abundance of helium with respect to hydrogen and keeping the rest of the elements in fixed proportion to each other while varying their absolute abundances by factors of 2 between models. Since the nucleogenic status of (either a primary or secondary element; Talbot and Arnett 1973) nitrogen is uncertain (see, for example, Alloin *et al.* 1979 and the review by Pagel and Edmunds 1981), sets of models with varying N/O ratios were computed; and since refractory grains may lock up C, Mg, and

TABLE 1  
PHYSICAL CONDITIONS OF REFERENCE MODEL

Shock velocity .....	106 km s <sup>-1</sup>
Postshock temperature .....	170000 K
Preshock conditions:	
Density .....	10 cm <sup>-3</sup>
Temperature .....	8200 K
Magnetic field .....	1 μG
Fractional ionization:	
H .....	1.00
He .....	1.00
Elemental abundances by number w.r.t. H:	
He .....	0.1
C .....	5 × 10 <sup>-5</sup>
N .....	5 × 10 <sup>-5</sup>
O .....	3 × 10 <sup>-4</sup>
Ne .....	6 × 10 <sup>-5</sup>
Mg .....	1 × 10 <sup>-5</sup>
Si .....	1 × 10 <sup>-5</sup>
S .....	7 × 10 <sup>-6</sup>
Cl .....	4 × 10 <sup>-7</sup>
Ar .....	6 × 10 <sup>-6</sup>
Absolute flux in Hβ in model .....	6.39 × 10 <sup>-5</sup> ergs cm <sup>-2</sup> s <sup>-1</sup> sr <sup>-1</sup>

Si, we also computed sets of models with varying C/O ratios but fixed C/Mg/Si ratios.

Consider first the behavior of the [O II] and [O III] lines as a function of abundance. Figure 7 shows the relationship between the λλ4959, 5007/Hβ ratio and the λλ3727, 3729/Hβ ratio for sets of models with varying O/N/C ratios. Tick marks represent factor of 2 changes in abundances of elements heavier than helium, the highest points corresponding to an oxygen abundance of 2.4 × 10<sup>-3</sup> by number with

respect to hydrogen. Note that the [O III] line ratios show a well-developed monotonic behavior with abundance, confirming it as a good abundance diagnostic. The range over which the [O II] line ratio varies is much more restricted. It shows a pronounced saturation effect at the high-abundance end and ambiguities dependent on the detailed abundance ratios. Overall, however, the theoretical trajectories in Figure 7 fit remarkably well on the observational trends of Figure 3 and show that oxygen abundances in observed SNRs (except for the SNR in IC 1613) lie between about 1.5 × 10<sup>-4</sup> and 1.2 × 10<sup>-3</sup>.

The saturation effect mentioned above was first found by Dopita (1977) and is caused by the fact that forbidden lines are the principal cooling agents in the recombination zone of the shock. Thus, since there is only a fixed amount of energy available for radiation in this zone, the combined emissions of the principal cooling agents C I], [C II], C II], C II, [N I], [N II], [O I], [O II], [Ne II], [Mg I], Mg II, Si I], [Si II], Si II], Si II, and S II] must be in constant ratio with the hydrogen Balmer lines, which arise mainly by recombination-cascade. This is confirmed by our models, and the saturation effect determines the maximum abundance to which the above lines retain their usefulness as abundance diagnostics. The [O II] lines are particularly bad in this regard, since they dominate the cooling in the recombination zone, and the oxygen ionization is locked to that of hydrogen by charge-exchange. As a result, they are *almost never* useful for abundance diagnostics. Saturation occurs at Z(O) ≈ 2 × 10<sup>-4</sup>, and this explains why SNRs and H II regions give discrepant results at higher oxygen abundances (Blair, Kirshner, and Chevalier 1982).

Saturation is less severe for the [N II] or [S II] lines, and these can be used up to about Z(O) ≈ 6 × 10<sup>-4</sup> (Fig. 8).

TABLE 2  
PRINCIPAL EMISSION LINES IN THE REFERENCE MODEL

Species .....	C II	N II	C III	O I]	O VI	C II	S IV	N II	S III	N I	Si III	O V]
λ (Å) .....	904	916	977	991	1035	1037	1068	1085	1197	1200	1206	1218
Rel. flux <sup>a</sup> .....	84.0	97.7	320	45.8	...	38.5	0.2	85.3	0.4	1.0	30.5	0.2
Species .....	N V	S II	Si III	Si II	C II	O I]	S IV]	Si IV	O IV]	N IV]	C IV	O III]
λ (Å) .....	1241	1255	1262	1263	1335	1358	1398	1398	1403	1486	1549	1664
Rel. flux <sup>a</sup> .....	0.2	0.5	22.6	9.4	186	2.0	3.8	34.8	5.0	8.3	48.9	70.4
Species .....	S III]	N III]	Si III]	C III]	N II]	[O III]	C II]	Si II]	[O II]	Mg II	C I]	[N I]
λ (Å) .....	1699	1748	1892	1909	2140	2321	2326	2335	2470	2800	2966	3466
Rel. flux <sup>a</sup> .....	1.3	10.4	65.4	143	28.4	3.2	76.6	30.6	8.4	34.2	13.5	0.4
Species .....	[O II]	[O II]	[Ne III]	[Ne III]	Hε	[S II]	[S II]	Hδ	Hγ	[O III]	[Mg I]	[Ar IV]
λ (Å) .....	3726	3729	3869	3967	3970	4069	4076	4101	4340	4363	4565	4711
Rel. flux <sup>a</sup> .....	414	483	37.3	11.1	15.3	17.7	5.8	25.1	45.9	12.5	54.8	4.8
Species .....	[Ar IV]	Hβ	[O III]	[O III]	[N I]	[Cl III]	[Cl III]	[O I]	[N II]	[O I]	[S III]	[O I]
λ (Å) .....	4740	4861	4959	5007	5199	5517	5537	5577	5755	6300	6312	6364
Rel. flux <sup>a</sup> .....	3.6	100	49.5	145	27.2	1.4	1.0	0.3	7.2	54.0	0.9	16.8
Species .....	[N II]	Hα	[N II]	[S II]	[S II]	[Ar III]	[O II]	[O II]	[Ar III]	[Cl II]	[S III]	[Cl II]
λ (Å) .....	6548	6563	6584	6716	6731	7136	7320	7330	7751	8577	9069	9123
Rel. flux <sup>a</sup> .....	52.4	302	154	137	124	15.8	29.2	22.9	3.8	2.2	3.0	0.6
Species .....	[S III]	[S II]	[S II]	[S II]	[N I]	He I	[Ar II]	[Ar III]	[Ne II]	[Ne III]	[S III]	[Ar III]
λ (μm) .....	0.952	1.031	1.034	1.037	1.040	1.08	8.00	8.99	12.5	15.5	18.9	21.8
Rel. flux <sup>a</sup> .....	7.3	7.8	3.5	1.5	2.1	10.4	38.8	6.8	105	5.6	2.2	0.4
Species .....	[S III]	[Si II]	[Ne III]	[O III]	[O I]	[O III]	[S IV]	[N II]	[O I]	[C II]	[N II]	H
λ (μm) .....	33.6	34.8	35.2	51.7	63.1	88.2	105	121	147	156	205	(2q)
Rel. flux <sup>a</sup> .....	2.8	269	0.6	42.	31.0	4.1	0.1	2.0	2.4	7.9	0.3	1860

<sup>a</sup> Flux relative to Hβ = 100.00.

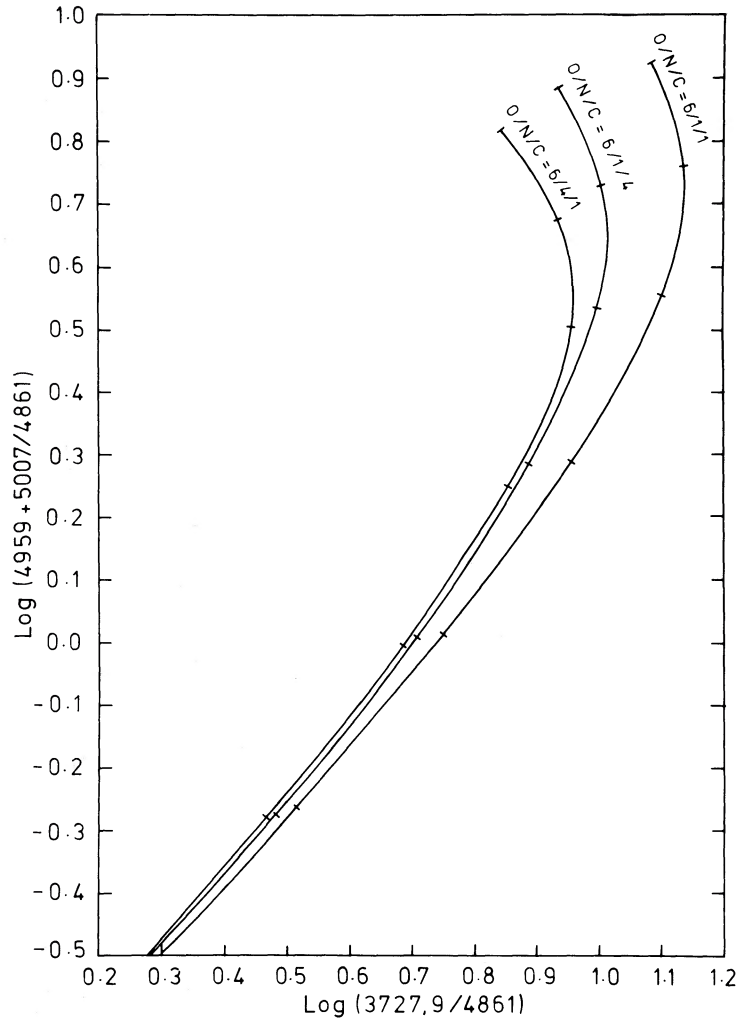


FIG. 7.—Theoretical trajectories of variable abundance models on a  $[O \text{ II}]/H\beta$  vs.  $[O \text{ III}]/H\beta$  diagram (compare Fig. 2). Each tick mark represents a factor of 2 change in metallicity; the curves terminate at an oxygen abundance of  $2.4 \times 10^{-3}$  by number with respect to hydrogen.

The competition between the  $[O \text{ II}]$ ,  $[N \text{ II}]$ , and  $[S \text{ II}]$  lines is a problem. This means that an unambiguous N/S ratio cannot be determined from a diagram such as Figure 1 if we do not know the oxygen abundance. Figure 8 does show, however, that the absolute value of the  $\lambda\lambda 6548, 6584/\lambda 6563$  ratio determines an N/O ratio with no ambiguity for a given oxygen abundance. The same is true for the  $\lambda 6731/\lambda 6563$  ratio; namely, that this ratio determines an S/O ratio for a given O abundance (see Fig. 9).

The possibility that “unseen” coolants in the UV (e.g.,  $[C \text{ I}]$ ,  $[C \text{ II}]$ ,  $[C \text{ III}]$ ,  $[Mg \text{ II}]$ ,  $[Si \text{ I}]$ ,  $[Si \text{ II}]$ , and  $[Si \text{ III}]$ ) or in the infrared ( $[C \text{ II}]$ ,  $[O \text{ I}]$ ,  $[Ne \text{ II}]$ , or  $[Si \text{ II}]$ ) may influence visible line intensities should be considered. The effect would be that an increase in abundance of the elements giving rise to lines outside the visible range of wavelengths would lead to a weakening of the visible lines. Figure 9 shows that this effect is very weak. We have plotted a set of models in which the abundance ratios of C, Mg, and Si with respect to O are varied. A weakening is found at the highest abundance, but it amounts to less than 0.1 dex in the line ratio. This is a very fortunate

circumstance. If a high sensitivity to this effect was found, then the optical lines of SNRs would be of very little use in abundance diagnostics, since the species giving rise to the effect are precisely those we would expect to be locked up in refractory grains, if these exist in the postshock gas. A full abundance diagnostic would then have to await spectrophotometry in the far-UV.

Lines of higher excitation are generally more sensitive in abundance diagnostic studies. This is because collisional excitation of He II is the dominant coolant where this species is present in abundance. This gives rise principally to the  $\lambda 304$  line and the helium two-photon continuum, which together give a flux of the order of 100 times that of  $H\beta$ . Heavy elements therefore act as impurity atoms as far as their effect on cooling is concerned, and so, provided the zone of emission of a particular ion lies within the He II zone, the emergent line flux will scale as the ion abundance. Thus, the  $[O \text{ III}]$  lines scale well with abundance (Fig. 8). In Figure 10 we plot the  $\lambda\lambda 6548, 6584/\lambda 6563$  ratio against the  $\lambda\lambda 4959, 5007/\lambda 4861$  ratio. Saturation effects are not serious enough to lead

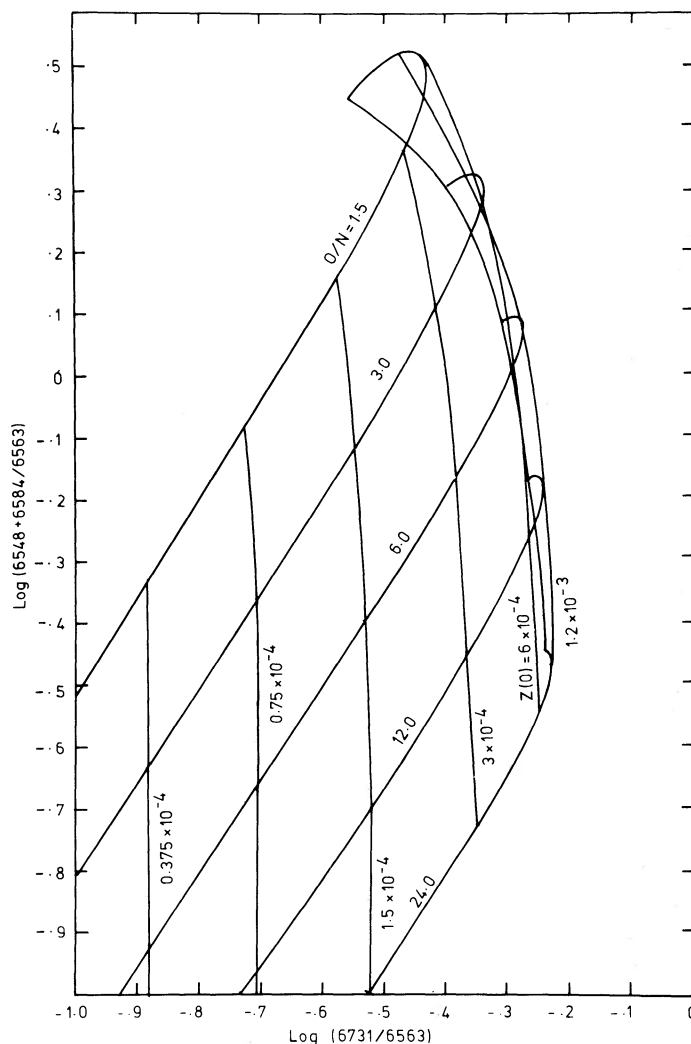


FIG. 8.—A grid of models with variable O/N abundance ratios and total metallicities (compare Fig. 1). The O/S abundance ratio is kept fixed at 42.8 by number. Note the saturation effect on the [S II] line as mentioned in the text.

to ambiguity over any of the computed abundance ranges, and so this plot can be used unambiguously to determine both O abundance and O/N ratio.

Comparison of Figure 10 and the data of Figure 3 reveals that theory and observation can be reconciled only if the nitrogen abundance varies over a larger factor than the oxygen abundance. The SNRs in the Magellanic irregular galaxies NGC 6822 and IC 1613 have oxygen abundances of  $0.5\text{--}1.5 \times 10^{-4}$  and O/N abundance ratios of 12–20. At the other extreme, RCW 103 in our Galaxy and the SNR BA 416 and 55 in M31 appear to have oxygen abundances in the range  $1.0\text{--}1.5 \times 10^{-3}$  and an O/N abundance ratio of the order of 3. This result is consistent with nitrogen being produced purely as a secondary nucleosynthesis element, but comparisons of one galaxy with another are dangerous, and we do not necessarily advocate this conclusion. An alternative hypothesis might be to suppose that oxygen is preferentially depleted onto grains (in the form of silicates) at high ISM abundance. However, the observational support for this is lacking. J. M. Shull (private communication)

reports that the *Copernicus* survey by R. C. Bohlin and others finds no evidence for either N or O depletion, and the level of a variation in the S/O ratio (below) also suggests no preferential depletion of oxygen. Some of these effects were found and discussed in an earlier paper (Binette *et al.* 1982), where alternative scenarios are also discussed.

There is little evidence that the O/S ratio is variable. This is clear from Figure 11, in which we plot the [O III]/H $\beta$  ratio against the [S II]  $\lambda 6731$ /H $\alpha$  ratio. Both observations and theoretical trajectories are shown. Within the errors of the theory and data, there is only a maximum of a factor of 2 variation in the O/S ratio over an abundance range of the order of 16. We conclude that, for extragalactic SNRs,  $O/S = 45 \pm 15$  by number. This result suggests that S, like O, is a primary element, and is at variance with the conclusions reached by observations of main-sequence F and G stars (Clegg, Lambert, and Tomkin 1981). These show that S varies as Fe, and that this variation is more rapid than that of O so that oxygen is relatively overabundant in the metal-deficient stars. It is interesting to note that our result does

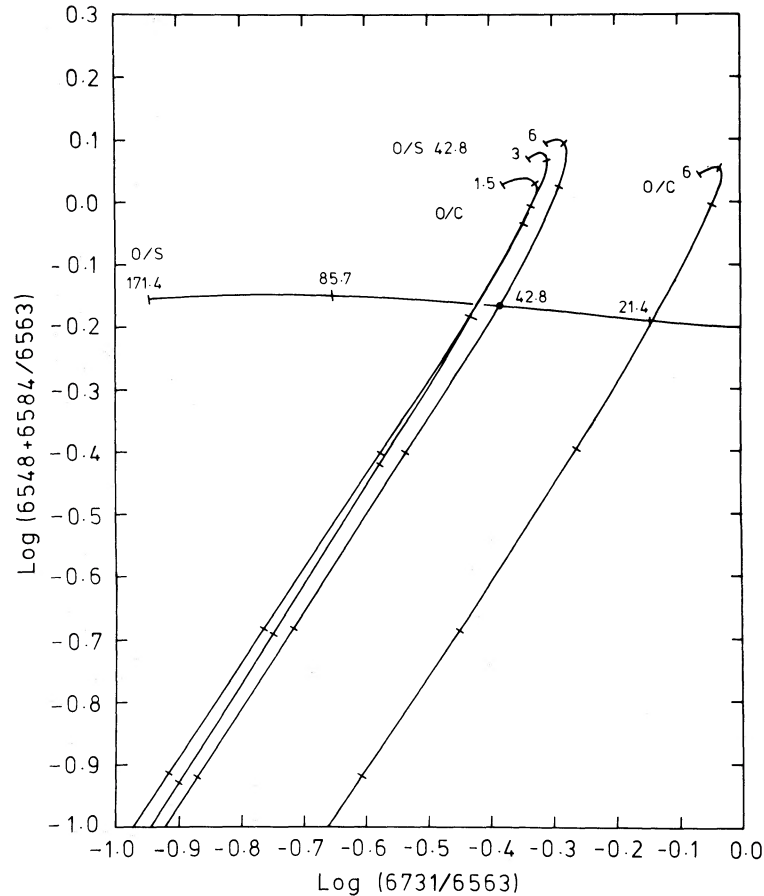


FIG. 9.—As Fig. 8, but the effect of varying the O/S ratio and O/C ratio is investigated

agree with data obtained from both H II regions and planetary nebulae (Kaler 1981). We must therefore conclude that some process, possibly occurring at the time of formation of the stars, is producing the change in O/S ratios. A plausible process is grain sedimentation in the protostellar cloud. This possibility is further supported by the puzzling discrepancy between oxygen abundances inferred from SNRs and H II regions in the solar neighborhood,  $Z(\text{O}) \approx 3 \times 10^{-4}$ , and the somewhat higher solar value. It is difficult to understand why local oxygen abundances inferred for SNRs and H II regions in the than that of the Sun, considering that additional processing of the interstellar medium must have occurred during the lifetime of the Sun. This mild depletion of oxygen, coupled to the stronger depletion of C, Mg, and Si seen in the Cygnus Loop (Binette *et al.* 1982), suggests that refractory grain materials are involved either in the sedimentation process mentioned above or by their survival in the post-shock gas. The latter possibility has theoretical support from the work of Cowie (1978) and Shull (1978). Shull showed that at a shock velocity of  $100 \text{ km s}^{-1}$ , not all grains are destroyed (about half for  $\text{MgSiO}_3$ ). Variable gas-phase abundances caused by grain destruction can be a useful addition to shock models, and this effect has been investigated by Shull, Seab, and McKee (1983).

### c) UV Abundance Diagnostics

Although UV spectra of high quality exist for only three remnants (Benvenuti, D'Odorico, and Dopita 1979, 1980; Raymond *et al.* 1980), it is clear that the advent of the Space Telescope and StarLab will lead to an explosive growth in this data base. In principle, the rich UV spectra of SNRs which show strong emission in many different stages of ionization can be used for accurate plasma diagnostics and abundance determinations for a wide variety of elements, including C, Mg, Si, and Al, which are not accessible from ground-based observations. Other elements such as S and N appear in many more stages of ionization, and this should also permit much more accurate measurement of their abundances.

In practice, we know already from both theory and observation that the resonance lines suffer from radiative transfer effects both in the shock structure itself and in the interstellar medium in the line of sight to the SNR (Raymond *et al.* 1980, 1981; D'Odorico *et al.* 1980). The latter effect is particularly severe for the low-excitation species, and the former affects all species and is very geometry dependent. Thus, resonance lines are not in general useful as abundance indicators, and for the rest of this section we restrict our

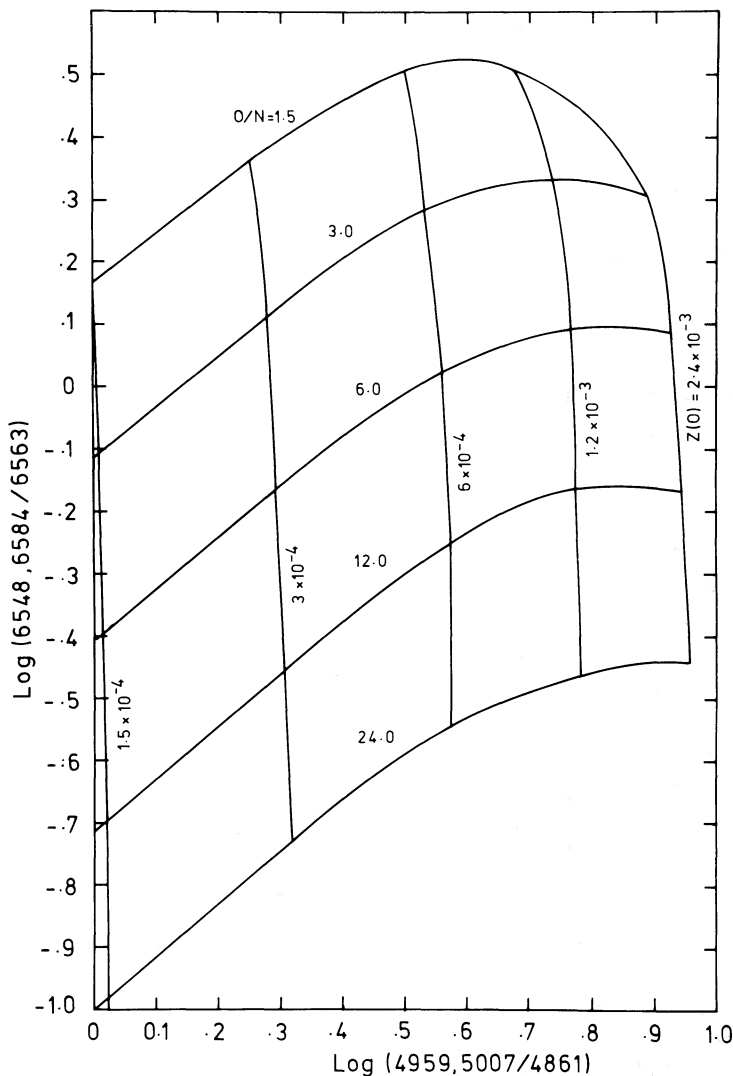


FIG. 10.—The grid of models of Fig. 8 shown on a diagram similar to Fig. 3. Note that both the  $[\text{N II}]$  and  $[\text{O III}]$  lines are excellent abundance indicators, and that line saturation is beginning to be apparent only at the highest metallicities.

attention to the intercombination lines, which suffer neither self-absorption nor collisional de-excitation for the physical conditions encountered in SNR shocks.

A radiative shock will have, at any chosen temperature in the postshock gas, an ionization structure dependent in part on the shock conditions and in part on the chemical abundance of the gas. It was demonstrated above that by the time the shocked gas flows through to the recombination zone of hydrogen, it retains little “memory” of the initial ionization conditions or shock temperature. However, in this zone the saturation effect limits the utility of low-excitation forbidden lines as abundance diagnostics.

Species of very high ionization state, on the other hand, will primarily be sensitive to shock conditions and therefore of little use for abundance diagnostics. As the shock velocity increases, the zone in which these species emit will extend until it becomes limited by recombinations from the next higher stage of ionization. The emission zone can then be said to be complete, and the ionization structure becomes

essentially invariant and independent of the shock conditions. When this point is reached, the relative flux in the line becomes constant with respect to other lines produced in complete ionization zones and depends only on the relative abundances of the species compared. A semiempirical formulation of this effect was given by Benvenuti, D’Odorico, and Dopita (1979). Figures 12 and 13 make this point clear. These figures correspond to the models of Figures 5 and 6, described above, and demonstrate the velocity-dependent effect on the flux of  $\text{C II}] \lambda 2326$ ,  $\text{C III}] \lambda 1909$ ,  $\text{O III}] \lambda 1664$ , and  $\text{O IV}] \lambda 1401$  with respect to  $\text{H}\beta$ . To an accuracy of 0.2 dex, the relative line fluxes of the first three species stabilize for shock velocities in excess of  $100 \text{ km s}^{-1}$ ; however, the  $\text{O IV}]$  line shows a tendency to stabilize only for a shock velocity in excess of  $150 \text{ km s}^{-1}$ .

The somewhat greater variability of the UV lines compared with the optical lines in the saturation zone is connected with the ionization of helium. In the range  $100\text{--}150 \text{ km s}^{-1}$ , helium lies between the singly and doubly ionized stages in the post-

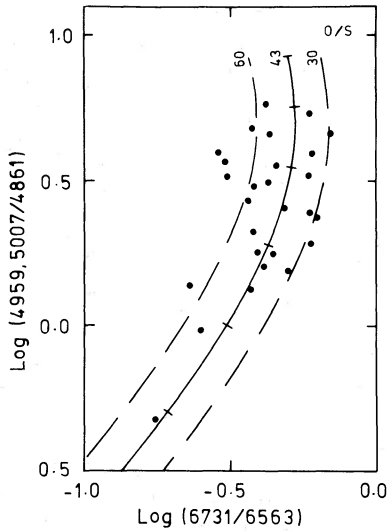


FIG. 11.—The theoretical and observational correlation between the [S II]  $\lambda 6731/H\beta$  and the [O III]  $\lambda\lambda 4959, 5007/H\beta$  intensity ratios. There is little evidence for a variability in the O/S ratio in this diagram. The theoretical lines terminate at an oxygen abundance of  $2.4 \times 10^{-3}$  by number with respect to hydrogen.

shock gas. Since collisional excitation of the singly ionized species is such an important cooling process, and materially affects the cooling time, the gradual conversion to full ionization at high velocity results in a slow change of ionization structure for a given element even when the ionization zone is complete in the sense described above.

In view of the saturation of lines of the neutral and singly

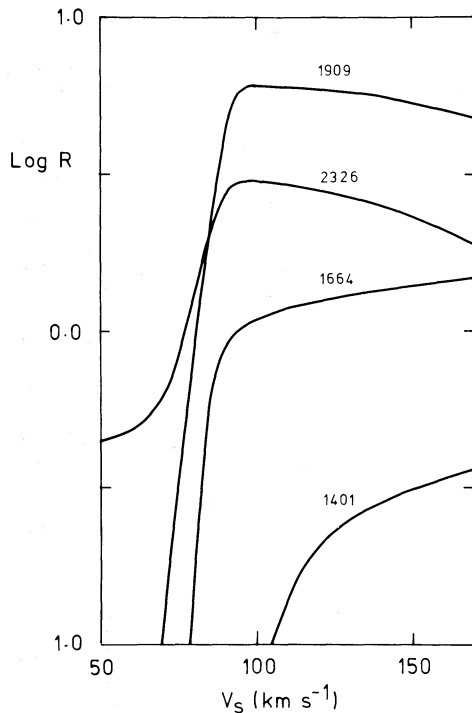


FIG. 12

FIG. 12.—Line ratios,  $R$ , with respect to  $H\beta$  in the fully self-consistent models of standard abundance (Table 1). The lines shown are the UV intercombination lines of C III]  $\lambda 1909$ , C II]  $\lambda 2326$ , O III]  $\lambda 1664$ , and O IV]  $\lambda 1401$ .

FIG. 13.—As Fig. 12 but for fixed pre-ionization (all elements singly ionized). Again (compare Figs. 5 and 6), the curves are scarcely distinguishable for  $V_s \geq 105 \text{ km s}^{-1}$ .

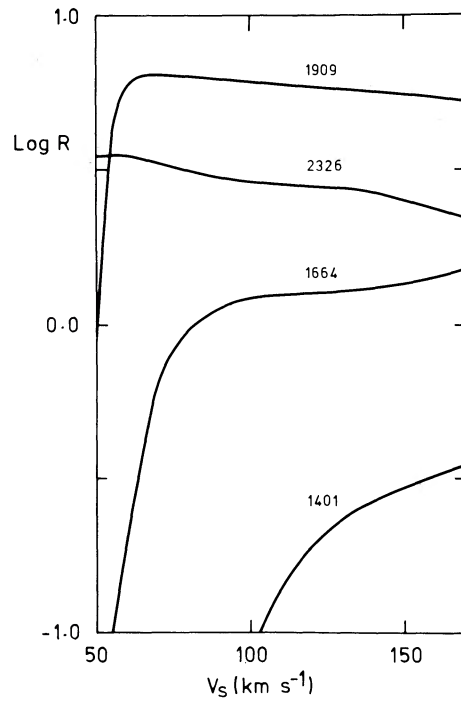


FIG. 13

ionized species, on the one hand, and the sensitivity of the highly ionized species to shock conditions on the other, we argue that intercombination lines of species of intermediate ionization give the best abundance diagnostics.

In Figure 14 we plot the relative fluxes of C III]  $\lambda 1909$  and O III]  $\lambda 1664$  with respect to  $H\beta$ . The sets of models used, with varying metallicity and O/C ratio, are the same used in preparation of the optical abundance diagnostic plots. Note that saturation effects are very weak and apparent only at the highest abundance, and that, if the shock velocity is high enough, these lines can give both an oxygen abundance and an O/C abundance ratio without ambiguity. Similar results apply for Si using the Si III]  $\lambda 1898$  line (Fig. 15) and for N using the N III]  $\lambda 1746$  line (Fig. 16).

Lines of higher excitation may be used, if shock velocities are high enough, since their behavior with abundance is very regular. Figure 17 illustrates this for the flux ratios with respect to  $H\beta$  of N IV]  $\lambda 1486$  and O IV]  $\lambda 1401$ .

#### IV. A METALLICITY INDEX

Since, in the optical wavelengths, the [O III], [N II], and [S II] lines are each primarily sensitive to the chemical abundances of the respective elements, a greater sensitivity could be achieved by multiplying together their flux ratios with respect to adjacent Balmer lines. We therefore define a metallicity index,  $M$ , by

$$\log M = \log \left( \frac{6731}{6563} \right) + \log \left( \frac{6548 + 6584}{6563} \right) + \log \left( \frac{4959 + 5007}{4861} \right).$$

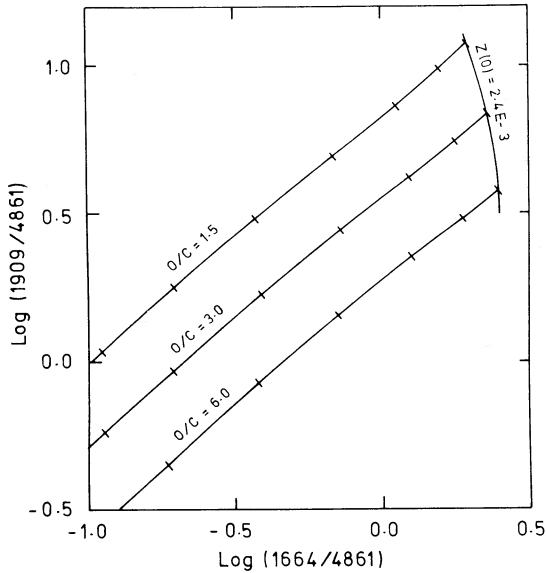


FIG. 14.—The theoretical correlation between the O III]  $\lambda 1664$  and C III]  $\lambda 1909$  lines with respect to  $H\beta$ . Tick marks represent a factor of 2 change in metallicity (increasing to the right). These lines are excellent abundance indicators. More exact wavelengths for all lines are given in Table 2.

If each line ratio were equally sensitive to abundance, then  $\log M$  should depend only on the sum of the logarithmic abundances of N, O, and S. To produce a quantity proportional to the “metal” abundance, we define an abundance,  $A$ , by

$$\log A = 0.8 + \frac{1}{3} \left[ \log \left( \frac{N}{H} \right) + \log \left( \frac{O}{H} \right) + \log \left( \frac{S}{H} \right) \right];$$

the additive factor 0.8 is arbitrary and is chosen so that, for a reasonable choice of  $N/H$  and  $S/H$ ,  $\log A \approx \log (O/H)$ .

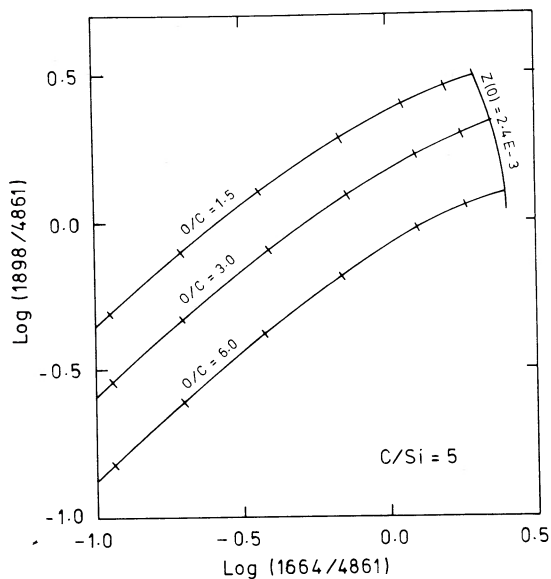


FIG. 15.—As Fig. 14 but for the O III]  $\lambda 1664/H\beta$  ratio and the Si III]  $\lambda 1898/H\beta$  ratio.

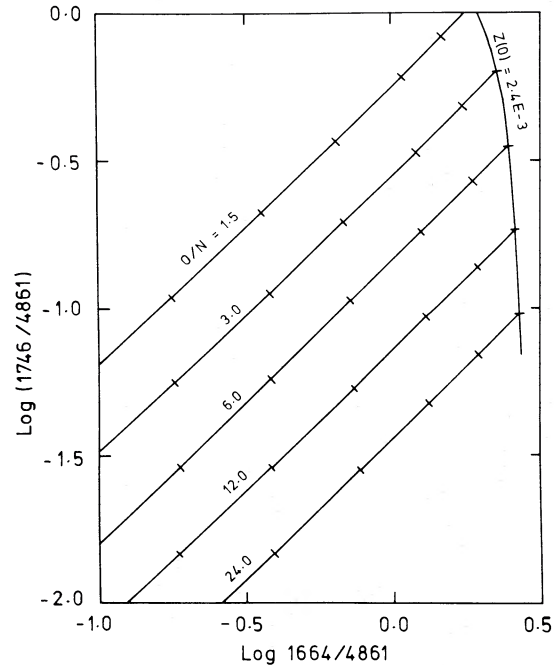


FIG. 16.—As Fig. 14 but for the O III]  $\lambda 1664/H\beta$  ratio and the N III]  $\lambda 1746/H\beta$  ratio.

With this choice of  $\log M$ ,  $\log A$  we plot the theoretical values for each of our models in Figure 18. The close clustering of points shows that a relation does indeed exist, and that a measure of  $\log M$  in a spectrum will give a ready estimate of the metallicity of the material passing through the shock, to an accuracy of the order of 0.2 dex. For  $\log A \gtrsim -3.2$ , saturation

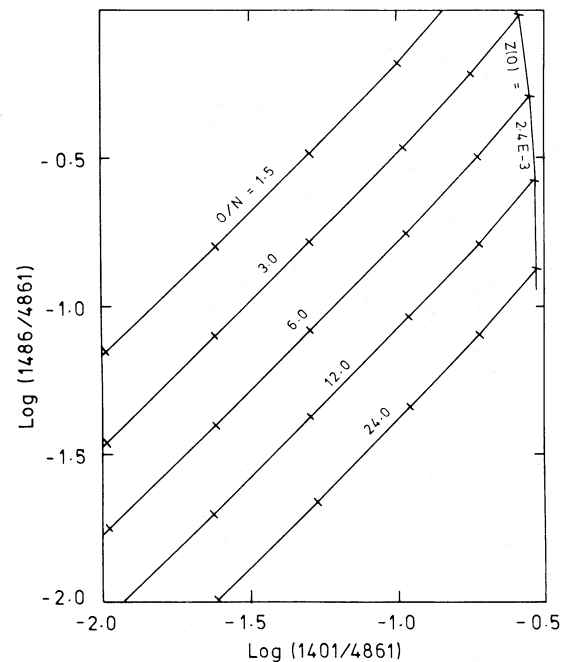


FIG. 17.—As Fig. 14 but for the O IV]  $\lambda 1401/H\beta$  ratio and the N IV]  $\lambda 1486/H\beta$  ratio. This is for a shock velocity of  $106 \text{ km s}^{-1}$ ; Figs. 12 and 13 should be used to transform to other shock velocities.

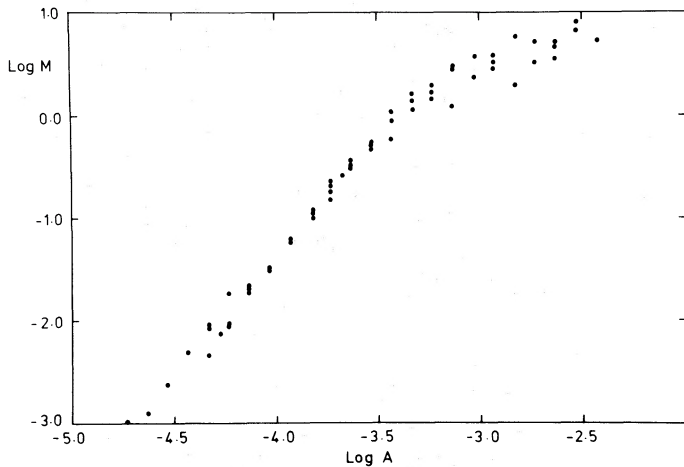


FIG. 18.—The metallicity index,  $M$ , plotted against the transformed abundance,  $A$ , defined in § IV. Each model is represented as a point showing the relatively small scatter between  $M$  and  $A$ .

effects become important, and sensitivity is lost when  $\log A \gtrsim -2.7$ .

On the basis of this index, we reexamine the data on M31 for an abundance gradient. Blair, Kirshner, and Chevalier (1981, 1982) find evidence for a gradient in N but not in O or S from their SNR observations. This result does not agree with the H II regions, which do show a regular O abundance gradient. We now know, from the above discussion, that saturation in the [O II] lines is a serious effect and can account for the discrepancy between the SNR and H II region results.

Since the simplest “one-zone” models of galactic chemical evolution predict a linear decline in the logarithmic metal abundance with galactocentric radius, and since the results for

H II regions are usually presented in this form (Pagel and Edmunds 1981), we plot in Figure 19 the  $\log A$  derived from the observed metallicity index against galactocentric distance for M31. Error bars are proportional to the scatter on the  $\log M/\log A$  relationship. The data are consistent with an abundance gradient of  $-0.05 \pm 0.02$  dex  $\text{kpc}^{-1}$ , a figure very similar to that found for SNRs in our Galaxy (Binette *et al.* 1982). Two points, corresponding to the regions BA 337 and BA 370, are clearly discrepant. These regions may be shock-excited by low-velocity shocks because the [O III] lines are so weak. However, they are also characterized by somewhat weak [S II] lines for their galactocentric distance, and we think it more likely that they are in fact low-excitation H II regions.

The abundance gradient for M33, derived in a similar manner from the observations of Dopita, D’Odorico, and Benvenuti (1980), is quite different (Fig. 20). Although the data show a pronounced [N II]/[S II] gradient, there is very little evidence of an abundance gradient out to 3 kpc on the basis of Figure 20, and the two outermost points show a dramatic drop. If one insisted on making a linear least squares fit to the points, a gradient of  $-0.08 \pm_{0.06}^{0.03}$  dex  $\text{kpc}^{-1}$  would be indicated. A small O abundance gradient in the inner 3 kpc was also found by Dopita, D’Odorico, and Benvenuti (1980), but since this occurred for near-saturation in the [O II] lines, it was not unambiguous.

#### IV. CONCLUSIONS

From our new grid of models, we conclude that for shock velocities in excess of about  $100 \text{ km s}^{-1}$ , the visible spectrum of a radiative shock depends primarily on the chemical abundances. This is borne out by the observational material, which with the theoretical models presented here enables relative abundances of N, O, and S to be determined and the

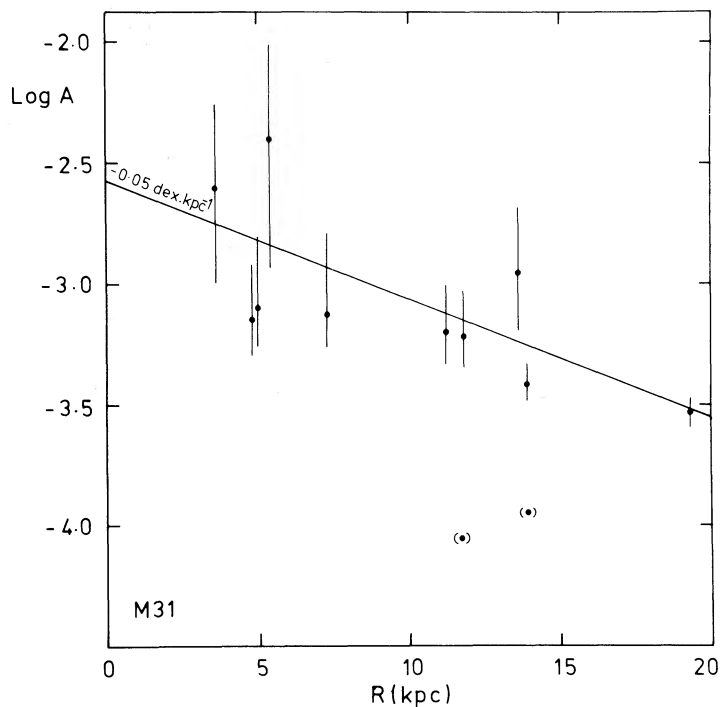


FIG. 19.—The M31 gradient in the transformed abundance  $A$  derived from the Blair, Kirshner, and Chevalier (1981, 1982) spectrophotometry

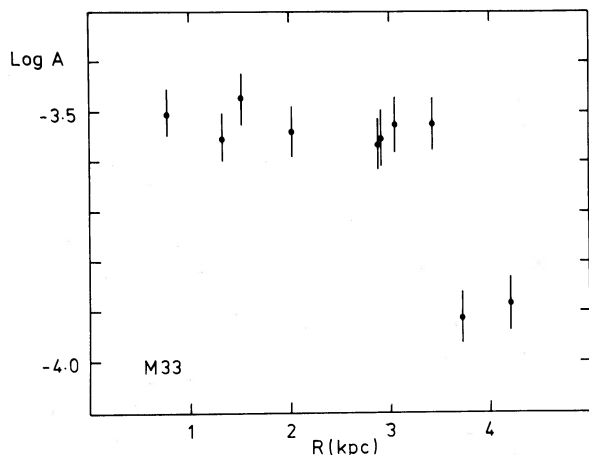


FIG. 20.—As Fig. 19 but for M33, using the Dopita, D'Odorico, and Benvenuti (1980) spectrophotometry.

size of the galactic abundance gradients to be measured. We find:

1. The oxygen/nitrogen abundance ratio depends strongly on oxygen abundance from around 15 at  $Z(\text{O}) = 10^{-4}$  to around 3 at  $Z(\text{O}) = 10^{-3}$ .

2. There is no evidence for a change in the oxygen/sulfur abundance ratio. It appears to be  $45 \pm 15$  in all objects observed.

3. The logarithmic chemical abundance gradient in M31 is  $-0.05 \pm 0.02$  dex  $\text{kpc}^{-1}$ , but the logarithmic abundance gradient in M33 cannot be characterized by a linear slope.

The ultraviolet intercombination lines have been investigated as diagnostic tools for measuring abundances in SNRs and proven to be, in general, more sensitive than the visible lines. Application of these techniques must await the advent of Space Telescope and StarLab.

S. D. wishes to acknowledge support by the Italian CNR whilst he was at the University of Padova.

#### REFERENCES

- Allen, C. W. 1973, *Astrophysical Quantities* (3d ed.; London: Athlone).
- Alloin, D., Collin-Souffrin, S., Joby, M., and Vigroux, L. 1979, *Astr. Ap.*, **76**, 200.
- Benvenuti, P., D'Odorico, S., and Dopita, M. A. 1979, *Nature*, **277**, 99.
- . 1980, *Ap. J.*, **238**, 601.
- Binette, L., Dopita, M. A., D'Odorico, S., and Benvenuti, P. 1982, *Astr. Ap.*, **115**, 315.
- Binette, L., Dopita, M. A., and Tuohy, I. R. 1983, *Ap. J.*, submitted (Paper II).
- Blair, W. P., Kirshner, R. P., and Chevalier, R. A. 1981, *Ap. J.*, **247**, 879.
- . 1982, *Ap. J.*, **254**, 50.
- Butler, S. E., and Raymond, J. C. 1980, *Ap. J.*, **240**, 680.
- Clegg, R. E. S., Lambert, D., and Tomkin, J. 1981, *Ap. J.*, **250**, 262.
- Cowie, L. L. 1978, *Ap. J.*, **225**, 887.
- Cox, D. P. 1972, *Ap. J.*, **178**, 143.
- Dennefeld, M., and Kunth, D. 1981, *A.J.*, **86**, 989.
- D'Odorico, S., Benvenuti, P., Dennefeld, M., Dopita, M. A., and Greve, A. 1980, *Astr. Ap.*, **92**, 22.
- D'Odorico, S., and Dopita, M. A. 1983, in *IAU Symposium 101, Supernova Remnants and Their X-Ray Emission*, ed. P. Gorenstein and J. Danziger (Dordrecht: Reidel), in press.
- D'Odorico, S., Dopita, M. A., and Benvenuti, P. 1980, *Astr. Ap. Suppl.*, **40**, 67.
- Dopita, M. A. 1976, *Ap. J.*, **209**, 345.
- . 1977, *Ap. J. Suppl.*, **33**, 437.
- . 1982, in *Supernovae: A Survey of Current Research*, ed. M. J. Rees and R. J. Stoneham (Dordrecht: Reidel), p. 483.
- Dopita, M. A., and Binette, L. 1983, in *IAU Symposium 101, Supernova Remnants and Their X-Ray Emission*, ed. P. Gorenstein and J. Danziger (Dordrecht: Reidel), in press.
- Dopita, M. A., D'Odorico, S., and Benvenuti, P. 1980, *Ap. J.*, **236**, 628.
- Dopita, M. A., Mathewson, D. S., and Ford, V. L. 1977, *Ap. J.*, **214**, 179.
- Draine, B. T. 1981, *Ap. J.*, **245**, 880.
- Fesen, R. A., Blair, W. P., and Kirshner, R. P. 1982, *Ap. J.*, **262**, 171.
- Kaler, J. B. 1981, *Ap. J.*, **244**, 54.
- Leibowitz, E. M., and Danziger, I. J. 1983, *M.N.R.A.S.*, in press.
- Ohtani, H. 1980, *Publ. Astr. Soc. Japan*, **32**, 11.
- Pagel, B. E. J., and Edmunds, M. G. 1981, *Ann. Rev. Astr. Ap.*, **19**, 77.
- Pradhan, A. K. 1978, *M.N.R.A.S.*, **183**, 89.
- Raymond, J. C. 1979, *Ap. J. Suppl.*, **39**, 1.
- Raymond, J. C., Black, J. H., Dupree, A. K., Hartmann, L., and Wolff, R. W. 1981, *Ap. J.*, **246**, 100.
- Raymond, J. C., Black, J. H., Hartmann, L., and Wolff, R. S. 1980, *Ap. J.*, **238**, 881.
- Ruiz, M. T. 1981, *Ap. J.*, **243**, 814.
- Shull, J. M. 1978, *Ap. J.*, **226**, 858.
- Shull, J. M., and McKee, C. F. 1979, *Ap. J.*, **227**, 131.
- Shull, J. M., Seab, C. G., and McKee, C. F. 1983, in *IAU Symposium 101, Supernova Remnants and Their X-Ray Emission*, ed. P. Gorenstein and J. Danziger (Dordrecht: Reidel), in press.
- Talbot, R. J., Jr., and Arnett, W. D. 1973, *Ap. J.*, **186**, 57.

PIERO BENVENUTI: ESA Villafranca, Satellite Tracking Station, Madrid, Spain

LUC BINETTE and MICHAEL A. DOPITA: Mount Stromlo and Siding Spring Observatories, Private Bag, Woden P.O., A.C.T. 2606, Australia

SANDRO D'ODORICO: European Southern Observatory, Garching-bei-München, FDR